# ENDOR Study of $VO^{2+}$-Imidazole Complexes in Frozen Aqueous Solution

**Charles F. Mulks, Burkhard Kirste, and Hans van Willigen***

*Contribution from the Department of Chemistry, University of Massachusetts at Boston, Boston, Massachusetts 02125.* *Received December 7, 1981*

**Abstract:** Complexes formed between the oxovanadium(IV) cation and imidazole, carnosine, and histidine have been studied with ENDOR. It is shown that the technique gives information on proton and nitrogen hyperfine coupling components as well as $^{14}N$ quadrupole splittings. The data provide insight into the geometric structure of the complexes. The results presented indicate that ENDOR studies of $VO^{2+}$ binding to more complex systems of biological interest (such as proteins) can be used to identify binding to histidine moieties. Furthermore, such studies could be of help in establishing the binding site geometry.

The oxovanadium(IV) ion ($VO^{2+}$) has been used in EPR studies of metal ion binding in a variety of systems of biological interest.[1] ENDOR studies of $VO^{2+}$ complexes randomly oriented in a rigid matrix[2-4] have demonstrated that this technique can provide valuable complementary data. With the aid of ENDOR, information is obtained on hyperfine and quadrupole tensor components of ligand nuclei. This may serve to identify ligands involved in metal ion binding and will give a more detailed insight into the structure of metal ion complexes than that provided by EPR studies alone.

Experience obtained in ENDOR studies of well-characterized $VO^{2+}$ complexes indicates that the analysis of spectra of systems of biological interest will require a base of ENDOR data on relevant model compounds. This consideration prompted us to make an ENDOR study of the complex formed between $VO^{2+}$ and imidazole (Im, I). The imidazole ring, as the histidine moiety,

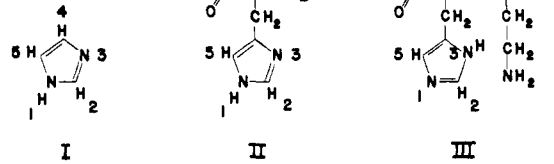

I II III

functions as a binding site for metal ions in a variety of molecules of biological interest.[5] Information on proton and nitrogen ENDOR spectra of the $VO^{2+}$-Im complex may make it possible to use the technique to identify metal ion binding to Im in proteins. Furthermore, the data may give information on the geometry of the binding site.

The salient points of the results presented in this paper are the following: (1) High-resolution $^1H$, $^{14}N$, and $^{15}N$ ENDOR spectra of $VO^{2+}$-Im and related complexes in frozen solution are readily obtained at temperatures above 77 K. (2) Values of hyperfine and quadrupole components derived from these spectra give information on the structure of the $VO^{2+}$-Im complex. For instance, the data indicate that four Im ligands are bound to the cation and that these ligands are oriented similarly. (3) A comparison of the ENDOR spectra from $VO^{2+}$-Im with those obtained from $VO^{2+}$-histidine (His, II) and $VO^{2+}$-carnosine (Car, III) establishes that the technique can be used to identify Im binding sites in more complex systems. (4) Changes in Im plane orientation, imposed for instance by geometric constraints of multidentate ligands (such as His), are reflected clearly in the proton as well as nitrogen ENDOR spectra. In systems of biological interest such changes also can be effected by substrate binding. It is evident that the possibility to study such effects is of considerable interest. (5) The absence or presence of axially coordinated $H_2O$ can be ascertained with ENDOR. In applications involving metal ion-protein complexes, this can convey information on the position of the cation.

Table I. Summary of EPR Data[a]

| | $g_{iso}$[b] | $g_z$ | $g_{xy}$ | $A_{iso}$,[b] $10^{-4}$ cm$^{-1}$ | $A_z$, $10^{-4}$ cm$^{-1}$ | $A_{xy}$, $10^{-4}$ cm$^{-1}$ |
|---|---|---|---|---|---|---|
| $VO(H_2O)_5^{2+}$ | 1.964 | 1.934 | 1.979 | 106.6 | 182.4 | 72.0 |
| $VO(Im)_4^{2+}$ | 1.971 | 1.952 | 1.981 | 91.1 | 162.1 | 57.4 |
| $VO(His)_n^{2+}$ | 1.973 | 1.955 | 1.980 | 85.4 | 156.4 | 54.5 |
| $VO(Car)_n^{2+}$ | 1.972 | 1.952 | 1.980 | 88.4 | 158.7 | 56.2 |
| $VO(thiazole)_n^{2+}$ | 1.966 | 1.940 | 1.980 | 99.9 | 170.9 | 65.0 |

[a] Experimental uncertainties: ±0.001 for $g_{iso}$ and ±0.002 for $g_z$ and $g_{xy}$, $\pm 0.5 \times 10^{-4}$ cm$^{-1}$ for the hyperfine values. [b] Isotropic values were determined from aqueous solution spectra recorded at room temperature.

The data reported here complement those obtained in previous magnetic resonance studies of the $Cu(Im)_4^{2+}$ complex.[6,7]

## Experimental Section

Imidazole, L-histidine, and L-carnosine from Sigma, perdeuterated (98%) imidazole ($ImD_4$, Merck), $^{15}N$-labeled (99%) imidazole ($Im^{15}N$, Prochem), and thiazole (Aldrich) were used without further purification. Partially deuterated imidazole samples (ImD, $ImD_2$, and $ImD_3$) were obtained through isotope exchange with $D_2O$ (and/or $H_2O$) using established procedures.[7,8] $VOSO_4 \cdot xH_2O$ (Alfa Inorganics) was used as received.

ENDOR samples were prepared by dissolving the appropriate amounts of $VOSO_4$ and ligand in a 2:1 $H_2O$/glycerol (or $D_2O$/glycerol-$d_3$) solvent mixture. The pH was adjusted with HCl or NaOH. Glycerol was added to ensure glass formation.[9] Experimental results show that the addition of glycerol effects a significant increase in signal to noise in the ENDOR spectra even though it may have no apparent effect on the rigid matrix EPR spectra. Glycerol addition does not appear to affect ENDOR line positions.

EPR and ENDOR spectra were recorded with a Varian E-9 X-band spectrometer equipped with a home-built ENDOR accessory. The ENDOR system has been described previously.[3,4] A Nicolet 1180E minicomputer interfaced to the EPR/ENDOR spectrometer was used for data collection and analysis. Magnetic fields were measured with an AEG NMR gaussmeter. DPPH was used as reference in $g$-value determinations. Measurements down to 100 K were performed with a variable-temperature accessory by using cold nitrogen gas. Measure-

(1) For a recent review, see: Chasteen, N. D. In "Biological Magnetic Resonance"; Berliner, L. J., Reuben, J., Eds.; Plenum Press: New York, 1981; Vol. 3.
(2) van Willigen, H. *Chem. Phys. Lett.* **1979**, *65*, 490.
(3) van Willigen, H. *J. Magn. Reson.* **1980**, *39*, 37.
(4) Mulks, C. F.; van Willigen, H. *J. Phys. Chem.* **1981**, *85*, 1220.
(5) For a review, see: Sundberg, R. J.; Martin, R. B. *Chem. Rev.* **1974**, *74*, 471.
(6) Mims, W. B.; Peisach, J. *J. Chem. Phys.* **1978**, *69*, 4921.
(7) Van Camp, H. L.; Sands, R. H.; Fee, J. A. *J. Chem. Phys.* **1981**, *75*, 2098.
(8) Lamotte, B.; Gloux, P. *J. Chem. Phys.* **1973**, *59*, 3365.
(9) Albanese, N. F.; Chasteen, N. D. *J. Phys. Chem.* **1978**, *82*, 910.

0002-7863/82/1504-5906$01.25/0 

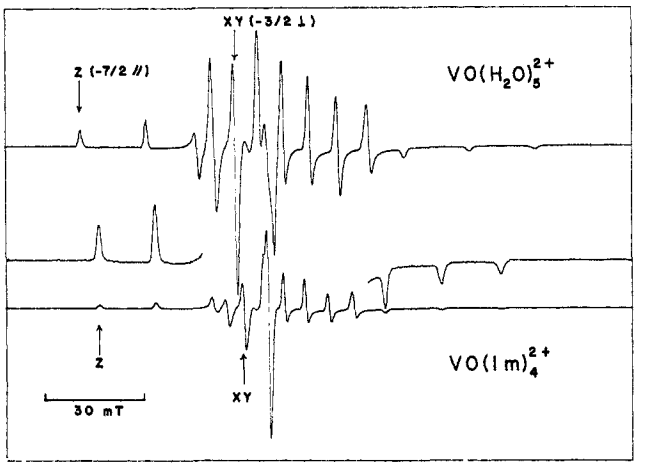


**Figure 1.** Frozen solution EPR spectra of $VO(H_2O)_5^{2+}$ (top) and $VO(Im)_4^{2+}$ (bottom) in $H_2O$/glycerol (2:1) at about 100 K. The field increases from left to right.

ments down to 4.2 K were performed with an Oxford Instruments ESR9 helium cryostat. Typical spectrometer settings used in recording the ENDOR spectra were as follows: temperature, ~100 K; microwave power, 20 mW; rf power, 200 W; FM, 10 kHz; FM deviation, ~100 kHz. ENDOR spectra are presented in the first derivative mode. Computer simulations were performed with the Cyber 175 computer of the University of Massachusetts. The simulations involve a calculation of eigenvalues and eigenvectors of the Hamiltonian matrix from which line positions and intensities are derived. In the case of powder spectra, this procedure is executed for a selected set of angles and the final spectrum is obtained by numerical integration. In all cases a Lorentzian line shape is assumed.

## Results

**EPR Data.** The rigid matrix EPR spectrum of a solution of $VO^{2+}$ ($2 \times 10^{-2}$ M) and Im (2 M) at pH ~ 7 is shown in Figure 1. The figure includes the spectrum obtained in the absence of Im. It is evident from the spectra and the data on $g$ and $^{51}V$ hyperfine components summarized in Table I that (around pH 7) the addition of excess Im to a solution of $VO^{2+}$ leads to the formation of a *single* $VO^{2+}$–Im complex. A comparison of the parameters in Table I with those reported for a variety of $VO^{2+}$ complexes[1] suggests that four Im molecules must be involved in the complexation. It is found that the Im concentration can be reduced by an order of magnitude before the presence of other species becomes evident in the EPR spectra in the form of a broad underlying resonance. This supports the conclusion that the spectrum shown in Figure 1 must be attributed to $VO(Im)_4^{2+}$. With excess Im (≥1 M), EPR and ENDOR spectra are not affected by pH changes within the range 5.5–8. At pH ~4 the EPR spectrum shows the presence of at least three species. At pH ~9 the presence of two distinct species is evident. The present study focused on the complex that gives rise to the spectrum shown in Figure 1.

Rigid matrix EPR spectra of solutions of $VO^{2+}$ ($2 \times 10^{-2}$ M) with a 5- to 10-fold excess of His, Car, or thiazole at pH ~7 also show the existence of a single vanadyl complex. Hyperfine and $g$ values derived from fluid solution and matrix EPR spectra of these complexes are listed in Table I. With the possible exception of the $VO^{2+}$–thiazole complex, the parameters indicate that four nitrogens are involved in $VO^{2+}$ binding.[1]

**Proton ENDOR.** The left hand side of Figure 2 shows a series of ENDOR spectra obtained with the magnetic field ($H$) set on the low-field turning point in the rigid matrix EPR spectrum (marked $z$ in Figure 1). With this field setting the ENDOR signal is due to molecules aligned so that the V=O axis (labeled $z$) is approximately along H[3]. Hence, the spectra give information on the hyperfine splitting components ($^iA_z$) along this axis for each set ($i$) of equivalent protons. For facilitation of the analysis of the spectrum due to $VO(Im)_4^{2+}$ in $H_2O$/glycerol (Figure 2a), spectra were obtained of a series of selectively deuterated complexes. These include the following (Figure 2 from top to bottom): (b) $VO(ImD_3)_4^{2+}$ in $H_2O$/glycerol, (c) the difference spectrum a – b, (d) $VO(ImD_2)_4^{2+}$ in $D_2O$/glycerol-$d_3$, and (e) $VO(ImD_3)_4^{2+}$ in $D_2O$/glycerol-$d_3$.

The right hand side of Figure 2 shows a set of spectra of the same systems obtained with the field set on the peak marked $xy$ in the EPR spectrum (Figure 1). For this field setting $H$ lies in

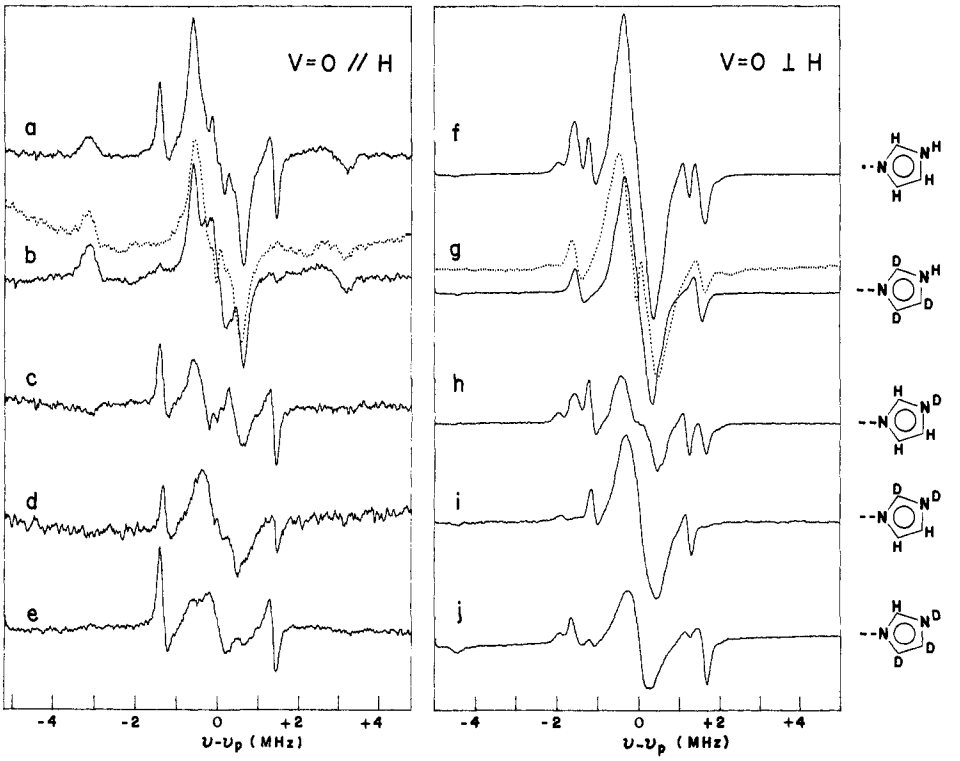


**Figure 2.** Proton ENDOR spectra of $VO(Im)_4^{2+}$ (~$2 \times 10^{-2}$ M), and a series of selectively deuterated complexes, in $H_2O$/glycerol (or $D_2O$/glycerol-$d_3$) matrix at about 100 K. Spectra on the left recorded with the magnetic field set on the peak marked z in Figure 1. Spectra on the right obtained with the $xy$ field setting. The dotted spectra are of $VO(H_2O)_5^{2+}$.

Table II. Summary of Proton ENDOR Hyperfine Couplings (in MHz)[a] in $VO(Im)_4^{2+}$

| | position | | | |
|---|---|---|---|---|
| | 2 | 4 | 1 | 5 |
| $A_z$ | 2.73 | 2.73 | 1.04 | 0.75 |
| $A_x$ | 3.37 | 2.51 | ≤0.8 | ≤0.8 |

[a] $A_z$ along V=O; $A_x$ in equatorial plane. The signs are not known; estimated uncertainties are ±0.01 and ±0.02 MHz for $A_z$ and $A_x$, respectively.

the plane ($xy$) perpendicular to the V=O axis.[3] Therefore, each set of equivalent protons can give rise to a two-dimensional powder pattern from which the values of the extremes of the hyperfine interaction ($^iA_x$ and $^iA_y$) in the plane can be derived. It should be noted that the $x$, $y$, and $z$ axes, in general, are not principal axes of hyperfine (or quadrupole) tensors and that $x$ and $y$ axes centered at different nuclei need not be colinear with each other.

Figure 2b shows that for $H\|z$ the water exchangeable protons give rise to two pairs of peaks with hyperfine splittings of 6.0 and 1.0 MHz and a peak centered at the free proton frequency ($\nu_p$). The latter may be due to bulk solvent protons. The position of the pair of peaks in the wings of the spectrum is virtually indentical with that found in the $VO(H_2O)_5^{2+}$ spectrum displayed by the dotted line in Figure 2b. Previous ENDOR studies of the aquo complex[3,10] show that these peaks are due to protons of an axially coordinated water molecule. The second pair of lines (splitting 1.0 MHz) is assigned to the proton bound to N1.

In the perpendicular spectrum ($H\perp z$) shown in Figure 2g the water exchangeable protons give rise to a pair of lines with a splitting of 3.14 MHz due to axially coordinated $H_2O$.[3] The hyperfine anisotropy in the equatorial plane is small[3,10] so that these peaks have single-crystal features. No evidence is found in either the $H\|z$ or $H\perp z$ spectra of the presence of equatorial $H_2O$ molecules. This is in accordance with the proposed stoichiometry of the $VO^{2+}$–Im complex. The anisotropy in the $xy$ plane of the NH proton hyperfine interaction is expected to give rise to a powder pattern in the spectrum shown in Figure 2g. In the first derivative representation two pairs of peaks should show up, marking the extremes of the hyperfine interaction in the plane. The positions of these pairs cannot be determined from the spectra. Judging from the H5 hyperfine data (vide infra), it is likely that both pairs fall under the $\nu_p$ peak. The spectra of $VO(ImD_3)$ and $VO(ImD_2)$ in $D_2O$/glycerol-$d_3$ (cf. Figure 2d,e) establish that for H2 $^2A_z$ = 2.73 MHz. The resonance peaks due to H4 and H5 in the $H\|z$ spectra cannot be assigned uniquely. Accepting the premise that $^4A_z > {}^5A_z$, one concludes that $^4A_z$ = 2.73 MHz (so that $^2A_z = {}^4A_z$) and $^5A_z$ = 0.75 MHz. The $H\perp z$ spectra (Figure 2f,h–j) show a weak pair of resonances (splitting 3.9 MHz) of which only the low-frequency peak is clearly evident. These peaks cannot be assigned to any of the imidazole protons since deuteration of the various positions does not affect their intensity. However, the peaks are absent in the spectrum of $VO^{2+}$ with perdeuterioimidazole in $H_2O$/glycerol (cf. Figure 2g). We must conclude that the resonances are due to some $VO^{2+}$-bound impurity introduced by Im. The prominent pair of lines shown in Figure 2i, with a splitting of 2.5 MHz, is sharply reduced in intensity upon deuteration of positions 4 and 5 (cf. Figure 2j). It is likely that these resonances are due to H4 so that $^4A_x$ = 2.5 MHz, while $^5A_x \leq 0.8$ MHz. A summary of the proton hyperfine data is given in Table II.

**$^{14}N,^{15}N$ ENDOR.** Figure 3 depicts the $^{14}N$ and $^{15}N$ ENDOR spectra obtained with $H\|z$ and $H\perp z$. The $H\|z$ spectrum of $VO(Im^{15}N)_4^{2+}$ (Figure 3b) shows the presence of two distinct nitrogens, each giving rise to a pair of peaks at $^1/_2|A_z| \pm \nu_n$, where $\nu_n$ is the nuclear Zeeman frequency. The hyperfine components $A_z(^{15}N)$ are found to be 9.05 and 9.89 MHz. The corresponding $^{14}N$ hyperfine components then must be 6.45 and 7.05 MHz, respectively. In the $^{14}N$ spectrum shown in Figure 3a, the two

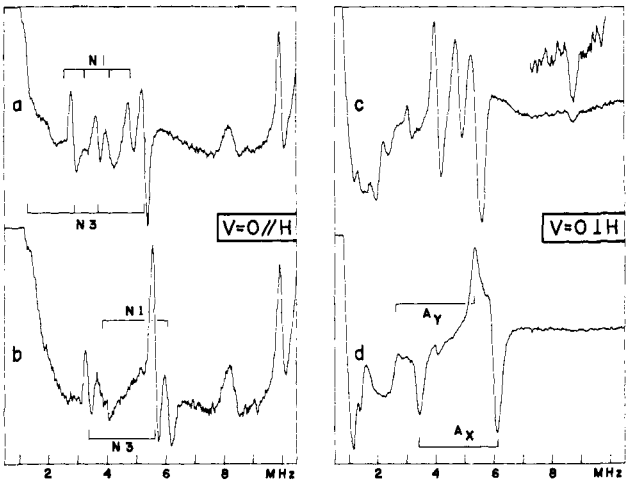


**Figure 3.** $^{14}N$ (a and c) and $^{15}N$ (b and d) ENDOR spectra from $VO(Im)_4^{2+}$ in $H_2O$/glycerol matrix at about 100 K. Spectra were obtained with the field set on the $z$ peak (a and b) or $xy$ peak (c and d) in the EPR spectrum (cf. Figure 1).

pairs of lines due to the two nitrogens are further split by the quadrupole interaction ($Q_z$):

$$\nu_{ENDOR} = {}^1/_2|A_z| \pm \nu_n \pm {}^3/_2Q_z$$

From the positions of the peaks one derives for one set of nitrogens $A_z(^{14}N)$ = 6.64, $Q_z$ = 0.80 MHz, and for the other $A_z(^{14}N)$ = 7.40, $Q_z$ = 0.23 MHz. The slight discrepancy between the experimental and $^{15}N$-derived $A_z(^{14}N)$ values may be due to second-order shifts introduced by the quadrupole interaction. Alternatively, it is possible that a slightly different range of molecular orientations is probed with the $z$-field setting. It is noted that the magnitude of the discrepancy resulting from these two sources cannot be estimated due to a lack of detailed information on the nitrogen hyperfine and quadrupole tensors.

The $H\perp z$ spectrum of $VO(Im^{15}N)_4^{2+}$ (Figure 3d) shows a pair of partly resolved lines between 5 and 6 MHz, a resonance around 3 MHz, and an indication of lines below 2 MHz, where baseline problems preclude a reliable analysis. The major features between about 2.5 and 6.2 MHz are attributed to a single set of equivalent $^{15}N$'s exhibiting a small hyperfine anisotropy in the $xy$ plane. The anisotropy gives rise to the powder line shape of the resonance around 6 MHz and, to a lesser extent, the resonance around 3 MHz. The asymmetric line shapes of these resonances may be due to the presence of resonance peaks of the second set of nitrogens. From the positions of the extremes of the resonance peaks one derives $A_x(^{15}N)$ = 9.6 and $A_y(^{15}N)$ = 8.0 MHz. According to the $^{15}N$ data, $A_x(^{14}N)$ = 6.8 and $A_y(^{14}N)$ = 5.7 MHz. Using these values as a starting point, we have tried to extract values for the $^{14}N$ quadrupole constants in the $xy$ plane from the $H\perp z$ spectrum shown in Figure 3c. The following set of data was found to account reasonably well for the prominent features in the experimental spectrum: $A_x$ = 7.00, $Q_x$ = 0.32, $A_y$ = 5.90, and $Q_y$ = 1.12 MHz. However, a computer simulation of the spectrum based on these parameters could not account for all the resonances observed below 4 MHz. Furthermore, there is some indication that additional resonances are buried under the prominent peaks between 2 and 6 MHz. These features could be due to the second set of nitrogens. The alternative that our choice of in-plane quadrupole parameters is in error cannot be excluded, however. As yet neither the $^{15}N$ nor the $^{14}N$ $H\perp z$ spectra have yielded reliable data for the second set of nitrogens. The $^{14}N\perp z$ spectrum (cf. Figure 3c) shows a weak, partially resolved, doublet around 8.8 MHz that can be assigned to $\Delta M_I$ = 2 transitions. These are weakly allowed due to admixture of $^{14}N$ nuclear spin states by the quadrupole interaction. To first order their positions are given by $|A_x(^{14}N)| + 2\nu_n$ and $|A_y(^{14}N)| + 2\nu_n$. From the positions of the $\Delta M_I$ = 2 lines, we derive $A_x(^{14}N) \simeq 6.8$ and $A_y(^{14}N) \simeq 5.9$ MHz. The values are in good agreement with those extracted from the $\Delta M_I$ = 1 region of the spectrum and the $^{15}N$ perpen-

(10) Atherton, N. M.; Shackleton, J. F. *Mol. Phys.* **1980**, *39*, 1471.

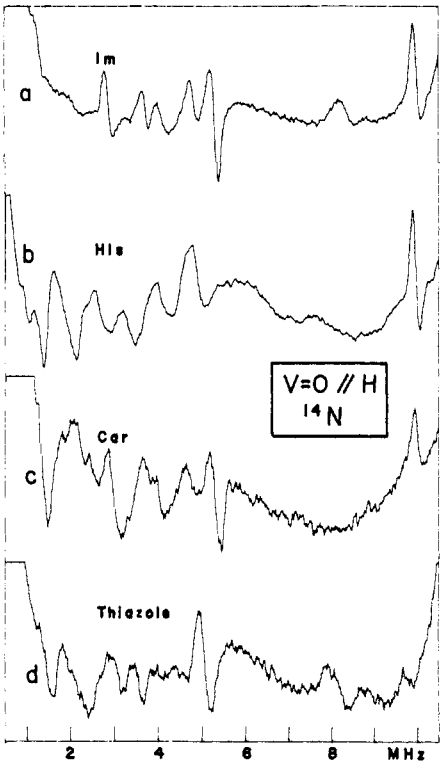


**Figure 4.** $^{14}N$ ENDOR spectra from (a) $VO(Im)_4^{2+}$, (b) $VO^{2+}$-histidine, (c) $VO^{2+}$-carnosine, and (d) $VO^{2+}$-thiazole, in $H_2O$/glycerol at about 100 K. Field set on the $z$ peak in the EPR spectrum (cf. Figure 1).

Table III. Summary of $^{14}N$ and $^{15}N$ Parameters (in MHz) in the $VO^{2+}$ Complexes

| ligand | position | $A_z$ | $Q_z$ |
|---|---|---|---|
| imidazole[a] | N1 | 7.40 (9.89)[b] | 0.23 |
| | N3 | 6.64 (9.05)[b] | 0.80 |
| histidine | N3 | 6.00 | 0.76 |
| carnosine | N1 | 7.10 | 0.24 |
| | N3 | 6.67 | 0.79 |
| thiazole | N3 | 6.5 | 0.7 |

[a] $^{15}N$ data show that $A_x(^{14}N) = 6.8$ MHz and $A_y(^{14}N) = 5.7$ MHz for one of the nitrogens. [b] $A_z(^{15}N)$ values.

dicular spectrum. The positions of the lines associated with "forbidden" transitions in the other electron spin manifold are given by $|A_x(^{14}N)| - 2\nu_n$ and $|A_y(^{14}N)| - 2\nu_n$. They are obscured by the strong peaks found around 5 MHz. Spectra were taken of vanadyl complexes of His, Car, and thiazole to explore the dependence of the $^{14}N$ parameters on structural changes. The well-characterized $H||z$ $^{14}N$ spectra of these complexes are shown in Figure 4 together with the corresponding spectrum of $VO(Im)_4^{2+}$. The spectrum of $VO^{2+}$-Car (Figure 4c) is very similar to that of $VO(Im)_4^{2+}$ (Figure 4a). For this complex the hyperfine and quadrupole splittings of two sets of $^{14}N$'s could be determined. For $VO^{2+}$-His the parameters of only one set could be determined, although resonance peaks due to a second set of nitrogens are evident. As expected, in the case of the thiazole complex the presence of only one set of nitrogens is evident. The $^{14}N$ parameters of the four complexes are summarized in Table III. The $H \perp z$ spectra of the His and Car complexes exhibit a set of well-defined, but as yet not interpreted, $^{14}N$ resonance peaks between 2.5 and 6 MHz. This feature is absent in the $H \perp z$ $^{14}N$ spectrum of $VO^{2+}$-thiazole which is mainly characterized by a broad resonance centered around 5 MHz.

## Discussion

First, some general comments can be made regarding the insight the ENDOR spectra provide into the structure of the $VO^{2+}$-Im complex. These observations serve to illustrate the potential value of the technique in the study of metal ion binding to the histidine moiety in proteins.

(1) As noted earlier, the spectra show no evidence of the presence of equatorial water molecules. This agrees with the stoichiometry of the complex suggested by the EPR data.

(2) On the other hand, the presence of an axially coordintaed $H_2O$ molecule is evident (cf. Figure 2, b and g). Judging from the hyperfine components given in Table II, the position of this molecule remains virtually unchanged upon going from $VO(H_2O)_5^{2+}$ to $VO(Im)_4^{2+}$. It is of interest to note that the ENDOR spectra of the complex formed between $VO^{2+}$ and excess His in aqueous solution (pH ~7) do not show axial $H_2O$ lines. It is evident that $VO^{2+}$ binding to N1 of the Im ring in His would leave the axial position exposed. Hence, the ENDOR data suggest metal ion binding to the Im N3 position. This could give rise to a geometry in which the axial position is blocked. Indeed, crystallographic studies[11-13] of metal ion–His complexes have shown that binding to N3, the amino nitrogen, and (possibly) the carboxyl group gives rise to a structure in which the cation is completely shielded from water of hydration. The $H||z$ ENDOR spectrum of $VO^{2+}$–Car does not show peaks that can be attributed to axial $H_2O$. However, this may be due to poor signal to noise. The $H \perp z$ ENDOR spectrum of this complex does show a slight deuteration effect in the frequency range where axial $H_2O$ peaks are expected. Studies[14-16] of the complex formed between $Cu^{2+}$ and excess Car show that around pH 7 the cation binds at the N1 position of the Im rings of four carnosine molecules. In this complex the axial position(s) can remain available for water of hydration. ENDOR spectra of the $Cu^{2+}$ complex in frozen aqueous solution provide evidence of the presence of one or two axial $H_2O$ molecules.[17] At the present time, the experimental data do not establish unequivocally whether or not the $VO^{2+}$–Car complex involves axially coordinated water.

(3) A crystallographic study of $Cu(Im)_4I_2$[18] shows that the four Im planes are oriented perpendicular to the equatorial plane. On the other hand, in $Cu(Im)_4SO_4$[19] one pair of Im rings makes an angle of 80° with the equatorial plane, whereas the other pair makes an angle of 29°. Apparently, the orientation of the Im rings can be affected by interactions with the axial ligands and neighboring molecules. The proton ENDOR spectra given in Figure 2 can be interpreted completely on the basis of a $VO(Im)_4^{2+}$ geometry in which *all four Im planes make the same angle with the equatorial plane.* A structure such as found for $Cu(Im)_4SO_4$[19] in principle would give rise to twice the number of peaks observed experimentally. A distribution of angles would give rise to much broader lines than observed experimentally. In contrast to the conclusion reached here, Van Camp et al.[7] recently proposed a spread of Im plane orientations for $Cu(Im)_4^{2+}$ in frozen aqueous solution. Their conclusion was based on the observation that the $H||z$ proton ENDOR spectrum only shows a broad line with little structure. However, the $H \perp z$ proton ENDOR spectra obtained by Van Camp et al.[7] do show well-resolved hyperfine splittings. This does not seem compatible with a spread in Im orientations. Furthermore, the observation of $^{14}N$ hyperfine structure in the rigid matrix EPR[7] argues against a disorder in the structure of the complex. In fact, both the $H||z$ and $H \perp z$ proton ENDOR spectra of $Cu(Im)_4^{2+}$ obtained in this laboratory[17] are well resolved. The spectra have not been analyzed in detail. However, it is evident that they reflect a well-defined geometry and that they are not incompatible with a unique Im ring orientation.

(11) Harding, M. M.; Cole, S. J. *Acta Crystallogr.* **1963**, *16*, 643.
(12) Kretsinger, R. H.; Cotton, F. A. *Acta Crystallogr.* **1963**, *16*, 651.
(13) Fraser, K. A.; Long, H. A.; Candlin, R.; Harding, M. M. *Chem. Commun.* **1965**, 344.
(14) Ihnat, M.; Bersohn, R. *Biochemistry* **1970**, *9*, 4555.
(15) Viola, R. E.; Hartzell, C. R.; Villafranca, J. J. *J. Inorg. Biochem.* **1979**, *10*, 281.
(16) Brown, C. E.; Antholine, W. E.; Froncisz, W. *J. Chem. Soc., Dalton Trans.* **1980**, 591.
(17) van Willigen, H.; Mulks, C. F., to be published.
(18) Akhtar, F.; Goodgame, D. M. L.; Rayner-Canham, G. W.; Skapski, A. C. *Chem. Commun.* **1968**, 1389.
(19) Fransson, G.; Lundberg, B. K. S. *Acta Chem. Scand.* **1972**, *26*, 3969.

The measured hyperfine components contain an isotropic contribution ($A_{iso}$) due to the Fermi-contact interaction and an anisotropic contribution due to the electron spin–nuclear spin dipole–dipole interaction ($A^D$). If the unpaired electron is confined virtually completely to the vanadium $3d_{xy}$ orbital, the dipole–dipole interaction between electron spin and proton ($i$) on the Im ring can be approximated by

$$^iA^D = g_e g_n \beta_e \beta_n (3 \cos^2 \theta_i - 1)/hr_i^3$$

Here $r_i$ is the V–$H_i$ distance and $\theta_i$ is the angle between V–$H_i$ axis and field direction. An effort was made to verify whether the $A^D$ contributions to the measured proton hyperfine components fit the point-dipole model. This is of interest, since, if that is the case, measurements of proton hyperfine components in $VO^{2+}$–protein complexes involving imidazole binding sites could provide quantitative data on binding site geometry.

With the aid of X-ray data,[18,19] the values of the components of $A^D$ along the V=O axis ($z$) and in the $xy$ plane were calculated for a series of Im plane orientations. Then we searched for an Im plane orientation for which the set of *measured* hyperfine components of the four protons could be interpreted satisfactorily in terms of the *calculated* $^iA^D$ components and $A_{iso}$ values. It turns out that the experimental data cannot be accounted for within the framework of this simple model. We conclude that spin delocalization does affect the hyperfine interactions. As a consequence, the experimental data cannot serve to give quantitative information on the Im plane orientation.

The $^{14}N$ and $^{15}N$ ENDOR spectra of $VO(Im)_4^{2+}$ (cf. Figure 3) for $H \| z$ show signals due to two sets of nitrogens. They may be due to N1 and N3 or to one of these exclusively. The latter interpretation implies two distinct rotation angles for the Im planes. This possibility is rejected for the following reason. The relatively large difference between the sets of $A_z$ and $Q_z$ values (cf. Table III) suggests that the orientations of the Im planes would have to differ substantially. Clearly, the presence of two distinct sets of Im planes should have been evident in the proton ENDOR spectra. The fact that $^{14}N$ ENDOR lines from only one set of nitrogens show up in the $H \| z$ spectrum of $VO^{2+}$–thiazole provides additional support for our interpretation.

For information on the assignment of the parameters to N1 and N3, and possibly the orientation of the Im rings, the measured quadrupole splittings were compared with published values for the quadrupole coupling constants in Im.[20,21] According to the literature, for N1, $Q_{z'z'} = 0.71$ and $Q_{x'x'} - Q_{y'y'} = 0.69$ MHz, and for N3, $Q_{z'z'} = 1.63$ and $Q_{x'x'} - Q_{y'y'} = 0.23$ MHz. Here $z'$ denotes the direction of the N–H or lone-pair orbital axis and $y'$ is the normal to the ring. The quadrupole coupling constant of the amino nitrogen (N1) appears to be relatively insensitive to complexation (with Zn, Cd, Cu), whereas for the imino nitrogen (N3) a decrease of up to 40% may be found.[7,21] Using the values given above and assuming that the rings are oriented perpendicular to the plane through four (coplanar) V–N bonds, we calculate $Q_z(N1) = +0.25$ and $Q_z(N3) = 0.70$ MHz. The $Q_z$ values for N1 and, to a lesser extent, N3 vary with rotation and tilt angle of the Im ring. Yet for reasonable geometries $|Q_z(N1)| \leq 0.4$ MHz so that we may conclude that the experimental data must be assigned as follows: N1, $A_z = 7.40$ and $Q_z = 0.23$ MHz; N3, $A_z = 6.64$ and $Q_z = (-)0.80$ MHz. Even with the assumption that the quadrupole parameters of N1 remain unchanged upon going from Im to $VO(Im)_4^{2+}$ not too much significance can be attached to the close correspondence between $Q_z$ calculated for the 90° conformation and the experimental value. A range of other conformations would give rise to a quadrupole splitting $|Q_z| = 0.23$ MHz. From the fact that the $^{14}N$ parameters for the $VO^{2+}$–Car complex are very similar to those of $VO(Im)_4^{2+}$ (cf. Table III), we conclude that the $VO^{2+}$–Im structure in the two complexes must be very similar. On the other hand, the $^{14}N$ spectra of $VO^{2+}$–His differ considerably from those of $VO^{2+}$–Car and $VO(Im)_4^{2+}$. The constraints imposed on the Im ring orientation due to the fact that His acts as a bidentate or tridentate[11-13] ligand probably account for this finding. The fact that the $^{14}N$ spectra apparently can serve as a probe of such changes in structure may prove useful in applications of the technique on more complex systems.

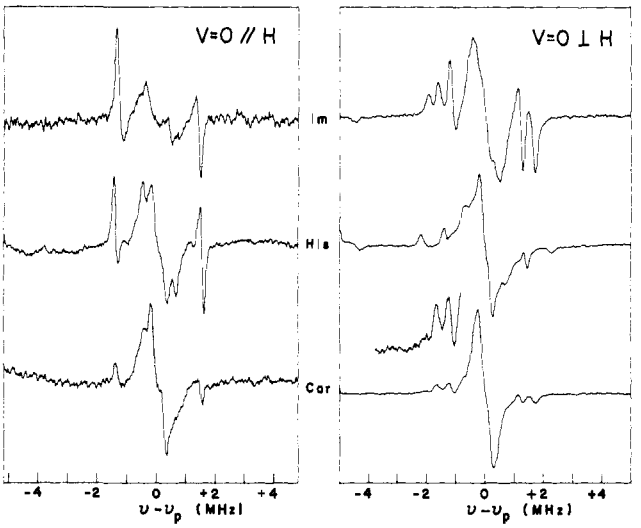


**Figure 5.** Proton ENDOR spectra from (top to bottom) $VO(Im)_4^{2+}$, $VO^{2+}$–histidine, and $VO^{2+}$–carnosine in $D_2O$/glycerol-$d_3$ at ~100 K. Spectra recorded with the magnetic field set on the $z$ (left) or the $xy$ (right) peaks in the EPR spectrum (cf. Figure 1).

From the $^{15}N$ and $^{14}N$ spectra of $VO(Im)_4^{2+}$ for $H \perp V{=}O$, only the hyperfine parameters of one set of nitrogens can be derived with certainty. The hyperfine coupling constants in the plane are $A_x(^{14}N) = 6.8$ and $A_y(^{14}N) = 5.7$ MHz. In the absence of a definitive analysis of the $^{14}N$ $H \perp z$ spectrum, there are no quadrupole data to guide us in the assignment of these $^{14}N$ hyperfine components to N1 or N3. The magnitudes of these parameters alone are not sufficient for an unequivocal assignment.

It is noteworthy that in $VO(Im)_4^{2+}$ the $z$ components of the hyperfine interactions of N1 and N3 are very similar in magnitude and, furthermore, that for N1 $A_z$ (7.4 MHz) is considerably larger than the hyperfine interaction (~2.5 MHz) with N1 in $Cu(Im)_4^{2+}$.[6,7] This may reflect the fact that in $Cu(Im)_4^{2+}$ the hyperfine interactions arise primarily as a result of $\sigma$ spin delocalization whereas in $VO(Im)_4^{2+}$ $\pi$ spin delocalization may play a significant role. A change in Im plane orientation upon going from $VO(Im)_4^{2+}$ to $VO^{2+}$–His would affect this $\pi$ spin delocalization contribution, and this could account for the pronounced change in the $^{14}N$ ENDOR spectra.

## Conclusion

In conclusion, we will address the question of the utility of ENDOR in studies of $VO^{2+}$ binding to Im moieties in more complex systems. As Figure 4 and the data in Table III illustrate, the ENDOR spectra give information on the hyperfine and quadrupole coupling components along the $z$ direction for the Im nitrogens. Further efforts, possibly aided by data from single-crystal studies, may resolve the question of the analysis of the $H \perp z$ $^{14}N$ spectra. Even now the $^{14}N$ spectra give information on changes in geometry as is exemplified in the series of $^{14}N$ spectra from $VO(Im)_4^{2+}$, $VO^{2+}$–His, and $VO^{2+}$–Car.

The similarity in geometry of the $VO^{2+}$–Im moiety in the $VO(Im)_4^{2+}$ and $VO^{2+}$–Car complexes on the one hand and the distinct structure that obtains apparently in $VO^{2+}$–His are clearly evident as well in the $H \perp z$ proton ENDOR spectra, given in Figure 5. The prominent doublet found in the $H \| z$ proton ENDOR spectra (cf. Figure 5, splittings of 2.73, 3.00, and 2.78 MHz for the Im, His, and Car complexes, respectively) also reflects structural changes. This characteristic pair of peaks may be useful in identifying binding to the Im moiety. In the spectrum from $VO^{2+}$–His these peaks have a smaller line width than in the spectra from the Im and Car complexes. According to our interpretation,

(20) Hunt, M. J.; Mackay, A. L.; Edmonds, D. T. *Chem. Phys. Lett.* **1975**, *34*, 473.
(21) Ashby, C. I. H.; Cheng, C. P.; Brown, T. L. *J. Am. Chem. Soc.* **1978**, *100*, 6057.

the doublet is due to two (slightly inequivalent) ortho protons in the latter two complexes, whereas it stems from a single ortho proton in $VO^{2+}$–His. The line-width change is in agreement with the proposed structures of the complexes.

Future theoretical work may provide a better understanding of the factors that affect the magnitudes of the hyperfine and quadrupole splitting components. Then the measured parameters could serve to provide us with a more detailed picture of the geometric structure of $VO^{2+}$–Im complexes. However, even in the absence of a more rigorous quantitative analysis, the data presented here make it evident that ENDOR can be of great value in giving a semiquantitative insight into $VO^{2+}$ binding site structure.

**Acknowledgment** is made to the donors of the Petroleum Research Fund, administered by the American Chemical Society, for support of this research. Financial support by the National Science Foundation (PRM-8100525, PCM-7903440) and Department of Energy (DE-AC02-81ER10911) for the purchase of equipment is gratefully acknowledged.

**Registry No.** $VO(Im)_4^{2+}$, 82871-04-3; $VO(H_2O)_5^{2+}$, 15391-95-4; L-histidine, 71-00-1; L-carnosine, 305-84-0; thiazole, 288-47-1.

# Chlorite Oscillators: New Experimental Examples, Tristability, and Preliminary Classification[1]

**Miklós Orbán,[2a] Christopher Dateo, Patrick De Kepper,[2b] and Irving R. Epstein***

*Contribution from the Department of Chemistry, Brandeis University, Waltham, Massachusetts 02254.* *Received March 16, 1982*

**Abstract:** Sustained oscillations are reported in the absorbance at 460 nm and in the potential of a Pt redox or iodide-sensitive electrode in a stirred-tank reactor (CSTR) containing solutions of chlorite, iodide, and an oxidizing substrate ($IO_3^-$, $Cr_2O_7^{2-}$, $MnO_4^-$, $BrO_3^-$) or chlorite, iodine, and a reducing substrate ($Fe(CN)_6^{4-}$, $SO_3^{2-}$, $S_2O_3^{2-}$). In addition to oscillations, a system containing chlorite, iodide, iodate, and arsenite can exhibit three different steady states, depending on initial conditions, for the same set of input flows, residence time, and temperature in the CSTR. Until a detailed mechanism for chlorite oscillators is developed, it seems reasonable to divide these systems into four classes: (A) the fundamental $ClO_2^-$–$I^-$ (or $ClO_2^-$–$I^-$–$IO_3^-$) oscillator, (b) $ClO_2^-$–$I^-$–oxidant systems, (C) $ClO_2^-$–$IO_3^-$ or (or $I_2$)–reductant systems, (D) iodine-free systems, e.g., $ClO_2^-$–$S_2O_3^{2-}$. A corresponding classification of bromate oscillators is discussed.

Oxyhalogen ions—bromate, iodate, or chlorite—are indispensable constituents of all known homogeneous isothermal chemical oscillators in solution. Although the first oscillating reaction discovered, the Bray–Liebhafsky reaction,[3] is an iodate system, the overwhelming majority of oscillators discovered to date contain either bromate or chlorite. The only other iodate oscillators developed since Bray's discovery in 1921 have been the related Briggs–Rauscher systems.[4,5]

Bromate oscillators have been by far the most thoroughly studied and characterized, notably the prototype Belousov–Zhabotinskii (BZ) system, which was discovered over 20 years ago.[6] Extensive bodies of experimental and theoretical work are now in remarkably good agreement[7] for the BZ reaction. Noyes[8] has recently formulated a generalized mechanism for bromate oscillators and has used this scheme to divide the known bromate oscillators into five distinct categories. While recent discoveries in this laboratory[1] have extended the range of bromate-driven oscillation beyond those categories treated by Noyes, the fundamental mechanism and notion of classification remain sound.

The study of chlorite oscillators is at a more primitive stage, since the first of these systems[9] was discovered only a year ago. However, progress has been remarkably swift, and the systematic classification and mechanistic description of chlorite oscillators now seem within reach. In this paper we report the discovery of several new chlorite-based oscillating reactions, summarize the

Table I. Chlorite Oscillators in a CSTR

| no. | system | special features | ref |
|---|---|---|---|
| 1 | $ClO_2^-$–$I^-$ | bistability between stationary and oscillating states | 10 |
| 2 | $ClO_2^-$–$I^-$–$IO_3^-$ | | this work |
| 3 | $ClO_2^-$–$I^-$–malonic acid | batch oscillation, spatial wave patterns | 11 |
| 4 | $ClO_2^-$–$I^-$–$Cr_2O_7^{2-}$ | | this work |
| 5 | $ClO_2^-$–$I^-$–$MnO_4^-$ | | this work |
| 6 | $ClO_2^-$–$I^-$–$BrO_3^-$ | bistability between stationary and oscillating states | this work |
| 7 | $ClO_2^-$–$IO_3^-$–$H_3AsO_3$ | first chlorite oscillator discovered | 9 |
| 8a | $ClO_2^-$–$IO_3^-$–$Fe(CN)_6^{4-}$ | | 13 |
| 8b | $ClO_2^-$–$I_2$–$Fe(CN)_6^{4-}$ | | this work |
| 9a | $ClO_2^-$–$IO_3^-$–$SO_3^{2-}$ | | 13 |
| 9b | $ClO_2^-$–$I_2$–$SO_3^{2-}$ | | this work |
| 10a | $ClO_2^-$–$IO_3^-$–$S_2O_3^{2-}$ | batch oscillation | 11 |
| 10b | $ClO_2^-$–$I_2$–$S_2O_3^{2-}$ | | this work |
| 11 | $ClO_2^-$–$IO_3^-$–$CH_2O{\cdot}HSO_2$ | | 13 |
| 12 | $ClO_2^-$–$IO_3^-$–ascorbic acid | | 13 |
| 13 | $ClO_2^-$–$IO_3^-$–$I^-$–malonic acid | batch oscillation | 11 |
| 14 | $ClO_2^-$–$I^-$–$IO_3^-$–$H_3AsO_3$ | tristability | this work |
| 15 | $ClO_2^-$–$S_2O_3^{2-}$ | first iodine-free chlorite oscillator | 12 |

(1) Part 11 in the series Systematic Design of Chemical Oscillators. Part 10: Orbán, M.; De Kepper, P.; Epstein, I. R. *J. Am. Chem. Soc.* **1982**, *104*, 2657–2658.

(2) Permanent addresses: (a) Institute of Inorganic and Analytical Chemistry, L. Eötvös University, H-1443, Budapest, Hungary. (b) Centre de Recherche Paul Pascal, Domaine Universitaire, 33405 Talence, France.

(3) (a) Bray, W. C. *J. Am. Chem. Soc.* **1921**, *43*, 1262–1267. (b) Liebhafsky, H. A. *Ibid.* **1931**, *53*, 896–911.

(4) Briggs, T. C.; Rauscher, W. C. *J. Chem. Ed.* **1973**, *50*, 496.

(5) Cooke, D. O. *Int. J. Chem. Kinet.* **1980**, *12*, 683–698.

(6) Belousov, B. P. *Ref. Radiat. Med.* **1959**, *1958*, 145–147.

(7) Field, R. J.; Noyes, R. M. *Acc. Chem. Res.* **1977**, *10*, 214–221. Noyes, R. M.; Field, R. J. *Ibid.* **1977**, *10*, 273–280.

(8) Noyes, R. M. *J. Am. Chem. Soc.* **1980**, *102*, 4644–4649.

(9) De Kepper, P.; Epstein, I. R.; Kustin, K. *J. Am. Chem. Soc.* **1981**, *103*, 2133–2134 (Part 2).

0002-7863/82/1504-5911$01.25/0 